Microporous and Mesoporous Materials 325 (2021) 111317

Contents lists available at ScienceDirect

Microporous and Mesoporous Materials

journal homepage: www.elsevier.com/locate/micromeso

Non-hydrolytic sol-gel synthesis of mesoporous iron-aluminum oxide and their properties in the oxidation of hydrocarbons by hydrogen peroxide

Gustavo Pimenta Ricci [a], Larissa Oliveira Garcia [a], Eduardo José Nassar [a], Shirley Nakagaki [b], João Felipe Stival [b], Zênis Novaes da Rocha [c], Miguel Angel Vicente [d,*], Raquel Trujillano [d], Alejandro Jiménez [d], Vicente Rives [d], Liziane Marçal [a], Emerson Henrique de Faria [a], Katia Jorge Ciuffi [a,**]

[a] Sol-Gel Group. Universidade de Franca, Parque Universitário, 201, 14404-600, Franca, SP, Brazil
[b] Bioinorganic and Catalysis Group, Departamento de Química, Universidade Federal do Paraná, Curitiba, PR, Brazil
[c] Instituto de Química, Universidade Federal da Bahia, Salvador, BA-40170-290, Brazil
[d] GIR-QUESCAT, Departamento de Química Inorgánica, Universidad de Salamanca, 37008, Salamanca, Spain

ARTICLE INFO

Keywords:
Porous iron-alumina
Oxidation reactions
Heterogeneous catalysts
Surfactants assisted synthesis

ABSTRACT

Iron-containing alumina materials were prepared by the non-hydrolytic sol-gel method in the presence of surfactants and their use as catalysts in the oxidation of hydrocarbons was studied. The solids were mesoporous, with large specific surface areas, > 250 m^2/g for the solids treated at 500 °C, depending on the surfactant used (cetyltrimethylammonium bromide, sodium dodecyl sulfate or hexadecylamine), and the calcination treatment applied (500 or 1000 °C). Iron was well distributed on the alumina surface, as confirmed by the EPR signals at 4.3 and 2.0 G and SEM imaging. The catalytic activity in the oxidation of cyclooctene, cyclohexane, and *n*-hexane was evaluated. After reaction for 48 h, the solid prepared with cetyltrimethylammonium bromide and calcined at 1000 °C showed a 25% conversion of cyclohexane with 51% selectivity to cyclohexanone. These were promising results, considering the mild reaction conditions, using a non-polluting oxidant at room temperature or 50–55 °C.

1. Introduction

Sustainable development addresses the urgent need to preserve the environment without leaving progress aside. As emphasized by Centi and Perathoner [1], for sustainable development to be achieved, sustainability must drive innovation. This requires an adaptation of the society, so that innovation capacity can be established as the basis of the competitiveness and the economy. The chemical industry being one of the areas that deserve attention for sustainable development to be attained, transition to a more sustainable chemistry demands that the chemical industry and its products are reconceptualized. Thus, sustainable development and green chemistry should serve as the basis during the search for alternative industrial processes that require milder conditions and generate the desired product selectively, while sharply decreasing waste production; if any waste is produced, it cannot be harmful and must be applicable in some other processes [2,3].

Selective oxidation of alkanes, alkenes, and aromatic hydrocarbons is one of the most important technologies to convert petroleum fractions into useful, better quality chemicals with a great commercial value [1,2,4,5]. The classical homogeneous catalysis for these reactions uses metallic salts, with low selectivity, requiring high temperature, energy, and pressure, and generating high amounts of hazardous waste. This scenario has aroused the interest of both academic and non-academic professionals in searching for efficient and environmentally friendly oxidation procedures that can be applied to develop sustainable processes for many kinds of oxidation reactions. Logically, the use of heterogeneous catalysts and green chemistry oxidizing hydrogen peroxide, with higher activity and selectivity, may be a great advantage compared to the classical procedure [1–7]. Recently, the design of new heterogeneous catalysts for selective oxidation under environmentally friendly conditions has attracted researchers' attention, and the sol–gel process has proven to be a powerful tool to prepare these catalysts [8–10].

Debecker et al. have published relevant reviews on the use of the non-hydrolytic sol–gel (NHSG) process to prepare heterogeneous

* Corresponding author.
** Corresponding author.
E-mail addresses: mavicente@usal.es (M.A. Vicente), katia.ciuffi@unifran.edu.br (K.J. Ciuffi).

https://doi.org/10.1016/j.micromeso.2021.111317
Received 31 May 2021; Received in revised form 16 July 2021; Accepted 20 July 2021
Available online 24 July 2021

catalysts [8,11–13]. This process offers several versatile routes that have already proven to be particularly useful for the preparation of various heterogeneous catalysts including TiO_2 [14], SiO_2–TiO_2 [15], V_2O_5–TiO_2 [16], MoO_3–SiO_2–Al_2O_3 [17], and Al_2O_3–SiO_2 [18], among others. Concerning the synthesis of alumina, the NHSG method has already proven to be efficient [19,20], especially when transition metal complexes are immobilized on the prepared supports [8,18–20]. By following the NHSG route and using ether or alcohol as oxygen donors, our research group has successfully obtained efficient catalysts; in particular, we have reported alumina matrixes with Fe(III) and Mn(III) porphyrins [21,22], Mn-salen [23], and Ni(II)-tetraaza [24] complexes. Compared to the hydrolytic route, the NHSG route has proven to be crucial to obtain efficient, stable, selective catalysts, mainly in the case of Fe(III) porphyrins [22]. The selected route influenced the final characteristics of the materials; and the structure, texture, and catalytic performance of all these catalysts heavily depended on the calcination temperature.

The NHSG route also proved to be quite interesting to construct isolated sites that mimic the active sites of biological enzymes. For instance, interesting biomimetic catalysts have been built by incorporation of iron onto alumina matrixes [25] and their catalytic applications have been also studied. Our aim was to develop a simple iron-based heterogeneous catalyst that would be as active as Fe(III) porphyrins, but avoiding the use of synthetic Fe(III) porphyrins themselves, which are obtained via complex, economically unviable syntheses. The synthesis of such Fe(III)–containing alumina catalysts was based on alkyl halide elimination via etherolysis/condensation between $AlCl_3$ and di-isopropyl ether in the presence of $FeCl_3$, followed by treatment of the obtained xerogel at different temperatures [21,22,25].

As underlined by Yang et al. [26], hierarchically porous structures that are found in living organisms like diatoms, leafs, and butterflies are key to inspiring the development of novel materials with optimal properties and performance, allowing its adaptation to constant environmental changes through long-term evolution, selectivity, activity, and resistance, as required by heterogeneous catalysts. Their exceptional properties are assigned to a functional adaptation of the structure at all hierarchy levels.

This methodology often leads to materials with low specific surface areas, which is disadvantageous for catalytic applications (only Vioux et al. [27] reported on materials with a specific surface area as large as 1043 m^2/g). A promising alternative looking for larger values of specific surface area is the use of surfactants during the synthesis of the materials; this will not only increase the surface area, but will also provide materials with ordered structures and well-defined active sites, essential characteristics for highly selective heterogeneous catalysts. The morphology of the catalyst can influence the distribution of the active sites. The presence of mesoporosity can enhance the selectivity and sometimes promote the re-oxidation; for instance, in cyclohexane oxidation by ironporphyrin immobilized on the interlayer space of kaolinite. The presence of active sites in confined spaces promotes the isolated site principle, as occurs in cytochrome P450 [28,29]. In this context, the use of cationic, anionic, or neutral surfactants to prepare hierarchical porous structures is a very interesting strategy to control the shape selectivity required for numerous industrial oxidation catalysts. Each sort of surfactant affords materials with different characteristics [30,31]. Thus, long-chain cationic *n*–alkyltrimethylammonium species (such as cetyltrimethylammonium, CTA) yields thermally stable porous phases, neutral *n*–alkylamines (like hexadecylamine, HDA) favor the synthesis of materials based on lamellar mesostructures or hexagonal micropores, and anionic dodecylsulfate (DS) leads to formation of mesoporous phases [30–32]. In all cases, the collapse of the ordered structure of the materials upon calcination to remove the surfactant is a key preparation step [31,33].

This work aims to prepare iron-containing alumina by the NHSG process in the presence of different surfactants. The solids will be fully characterized and later applied in the oxidation of hydrocarbons, such as cyclooctene, cyclohexane, and *n*-hexane.

2. Experimental

Analytical grade reagents purchased from Merck, Aldrich, Acros, or Mallinckrodt were used. The hydrogen peroxide solutions were from Peroxidos do Brasil Ltda. (70 wt% solution) or Chemical Base (50 wt% solution). Except for hydrogen peroxide, the solvents and reagents used in the oxidation reactions were purified on basic alumina (Merck, particle size 50–200 μm) columns.

2.1. Preparation of the catalysts

The preparation was carried out adapting the method described by Vioux's group [19,33], under conditions previously established by our research group [21–25]. The surfactants cetyltrimethylammonium bromide (CTAB), sodium dodecyl sulfate (SDS), and hexadecylamine (HDA) (see their structures and formulas in Fig. S1) were used for the first time in aprotic condensation routes.

Anhydrous aluminum chloride ($AlCl_3$, 3.0 g, 2.25×10^{-2} mol) and anhydrous iron (III) chloride ($FeCl_3$, 0.235 g, 1.449×10^{-3} mol) were dissolved in this order in anhydrous ethanol (10 mL). In a separate flask, a selected amount of surfactant was dissolved in 40 mL of anhydrous ethanol under magnetic stirring. The solutions were mixed with a Fe^{3+}/Surfactant/Al^{3+} molar ratio of 1:7.5:15. The resulting solution was then placed in a two-neck flask, and heated under reflux for 4h at 110 °C, under argon atmosphere and with magnetic stirring (the condenser was set up in an ultrathermostatic bath at –9 °C). The resulting gel was aged in the mother liquor under argon atmosphere at room temperature for 24 h. The solvent was then removed by drying at 100 °C, and portions of the solid were calcined in air at 500 or 1000 °C (temperatures selected from the thermogravimetric analysis) at a heating rate of 8 °C/min, and maintained 8 h at the final temperature. It was assumed that the entire amount of starting iron was incorporated into the final materials. The resulting solids were designated as FeAlO–S-T, where S stands for the surfactant used and T for the drying or calcination temperature (in °C).

2.2. Characterization and techniques

The thermal analyses were carried out up to 900 °C on a TA Instruments SDT Q600 Simultaneous TGA-DTA-DSC apparatus, at a heating rate of 10 °C/min under an O_2 flow of 100 mL/min.

The Fourier-Transform infrared (FT-IR) absorption spectra were recorded in a Bomem Michelson MB-100 spectrometer. The materials were analyzed from 4000 to 400 cm^{-1}, in the form of KBr pellets.

The powder X-ray diffraction (PXRD) analysis was accomplished on a Rigaku, model MiniFlex II diffractometer, operating at 40 kV and 30 mA (1200 W), using filtered Cu Kα radiation (0.15418 nm), from 2 to 65° (2θ), and at a scan speed of 2°(2θ)/min.

The N_2 adsorption-desorption isotherms (−196 °C) were recorded on a Micromeritics ASAP 2020 apparatus. Before analysis, the samples were degassed at 40 mmHg and 100 °C. The specific surface areas were determined by the BET method, and the total pore volume was obtained from the amount of N_2 adsorbed at a relative pressure of 0.95 [34]. The calculations for the pore size distribution were made by using the Barrett-Joyner-Halenda (BJH) method, which is the most efficient one for mesoporous materials [34].

The Transmission Electron Microscopy (TEM) analyses were performed using a Tecnai Spirit Twin in a Transmission Electron Microscope operating at 120 kV, at the Nucleus Research Platform, University of Salamanca, Spain. The Scanning Electron Microscopy (SEM) micrographs were recorded on a Zeiss microscope, model EVO 50. The microscope was coupled to an energy dispersive X-ray spectrometer (EDS) brand IXRF Systems, model 500 Digital Processing.

The electron paramagnetic resonance (EPR) spectra were obtained on a Bruker EMX Plus device, X-band (approximately 9.5 GHz). The

analyses were performed with powdered solid samples (0.040–0.070 g of dry material), at 25 °C.

The UV–Vis absorption spectra (solid state) were obtained on a Shimadzu spectrophotometer, model UV-2450, using $BaSO_4$ as a reference. When necessary, the spectra were deconvoluted by using the Origin® program (adjustment of multiple peaks by Gaussian or Lorentzian functions).

The Brønsted acid sites were quantified by thermal desorption of cyclohexylamine, as described by Breen et al. [35–37]. This method allows an easy estimation of the acidity of the samples and has given good results for clay materials. The solids were first equilibrated with cyclohexylamine vapor by locating 50 mL of this substance in a desiccator. Subsequently, 10 mg of each material were also introduced into the desiccator, which was closed and its internal pressure reduced with a vacuum pump, to facilitate cyclohexylamine evaporation. After 48 h, the samples were analyzed by TGA; cyclohexylamine removal between 240 and 420 °C is related to its desorption from Brønsted acid sites. Because this interval also involves the loss of other molecules, the mass referring to only cyclohexylamine was calculated by comparing the TG curves of the materials before and after steam-treatment of the material with this substance.

2.3. Standardization of hydrogen peroxide and preparation of anhydrous hydrogen peroxide

In some catalytic tests, anhydrous hydrogen peroxide (H_2O_2 in ethyl acetate) was used as oxidant. This solution was prepared by azeotropic distillation: 28 mL of 50 wt% H_2O_2 in water and 140 mL of ethyl acetate were added to a 250-mL round-bottom flask coupled to a "Dean-Stark" system bearing a tap in the collection tube. The flask was kept under agitation and heated in a silicone oil bath at 90 °C. The distilled liquid was collected. As water and ethyl acetate form an azeotropic mixture, the distillate consisted of these two solvents [38]. The residue, which consisted of a solution of H_2O_2 in ethyl acetate, was standardized by permanganometric titration, which revealed a concentration of 42 wt%.

Aqueous H_2O_2 solutions (50 and 70 wt%) were also standardized by permanganometric titration before use.

2.4. Catalytic tests

Cyclooctene, cyclohexane and *n*-hexane were used as substrates in the catalytic hydrocarbon oxidation tests. The tests were performed in 2-mL glass reactors containing screw caps and Teflon septa, under magnetic stirring; H_2O_2 was used as the oxidant.

The amount of Fe^{3+} ions in the catalysts was used to calculate the amounts of substrate and H_2O_2 that should be added to the reactors. The catalyst mass was 10 mg, which corresponded to 3.5 10^{-6} mol of Fe^{3+}.

For the catalytic tests, the Fe^{3+}/substrate/H_2O_2 molar ratios were 1:100:200 or 1:100:500. The reactions were conducted at 50–55 °C. Briefly, the cyclohexane oxidation tests involved 10 mg of catalyst, 5 μL of internal standard (*n*-butyl ether), 443 μL of solvent (1:1 dichloroethane/acetonitrile (v/v)), 40 μL of cyclohexane or 50 μL of *n*-hexane, and 160 μL of anhydrous (42 wt%) or aqueous (70 wt%) H_2O_2.

The results of the catalytic tests are given in terms of conversion: concentration (mol/L) of product(s)/initial concentration (mol/L) of substrate; the values are expressed in %.

2.5. Catalyst recycling

Three recycling cycles were carried out for the catalytic materials; each of them lasted 24 h. After each cycle was completed, the catalyst was recovered from the reaction medium by centrifugation, regenerated by drying in an oven at 100 °C for at least 6 h, and used in a new cycle.

2.6. Assessment of hydrogen peroxide deactivation

Non-productive decomposition of H_2O_2 was evaluated by permanganometric titration of the reaction medium after 24 h reaction. Given that gas chromatographic analysis allows substrate conversion to be quantified (it is believed [25] that the substrate:oxidant stoichiometry is 1:1), the amount of deactivated H_2O_2 can be calculated as the difference between the initial H_2O_2 concentration added to the reaction medium and the H_2O_2 concentration involved in substrate conversion.

2.7. Evaluation of the reaction mechanism

To assess the existence of a radical mechanism during the catalytic reactions, a test involving cyclooctene epoxidation was performed with sample FeAlO-CTAB-1000 in the presence of hydroquinone, a known radical scavenger [39,40].

To analyze the possible presence of cyclohexylhydroperoxide among the cyclohexane oxidation products, triphenylphosphine, a strong reducing agent, was added to the catalytic reaction after 48 h. In this way, any existing cyclohexylhydroperoxide would be reduced to cyclohexanol, as discussed by Shulpin et al. [41,42].

Products from the catalytic oxidation reactions were identified using a HP 6890 Series GC System gas chromatograph, with a flame ionization detector, equipped with a capillary column HPINNOWax-19091N-133 (polyethylene glycol, length 30 m, internal diameter 0.25 μm). The products were quantified using a calibration curve obtained with a standard solution, and the conversion was based on substrate (technical error: about ±1%).

3. Results and discussion

3.1. Characterization of the catalysts

Fig. 1 shows the powder X-ray diffractograms of the solids prepared from each surfactant, dried or calcined. The diffractogram of sample FeAlO-CTAB-100 corresponds to a mostly amorphous phase, but with small, sharp peaks at 2.27, 4.74, 7.19, 9.32, and 11.77° (2θ), which probably correspond to stacking of CTAB molecules. Upon calcination, these peaks disappeared, suggesting that the surfactant was removed. The solid obtained at 500 °C was amorphous, whereas the solid obtained at 1000 °C displayed sharp, intense peaks characteristic of a highly crystalline material, identified as the α-Al_2O_3 phase (JCPDS-71-1683 file).

When SDS was used as surfactant, the diagram of the dried solid showed two extremely weak peaks at low angle, suggesting that the surfactant molecules were stacked; the weak peaks between 20 and 30° (2θ) were also due to SDS. SDS was also removed under calcination, leading to an amorphous phase at 500 °C and to crystalline α-Al_2O_3 at 1000 °C. From the sharpness of the peaks, it can be concluded that FeAlO-SDS-1000 was roughly more crystalline than FeAlO-CTAB-1000, confirming that cationic and anionic surfactants played a fundamental role on alumina crystallization. The anionic surfactant might interact with Al^{3+} and Fe^{3+} ions via ionic bonds, resulting in smaller clusters than in the case of Fe–AlO-CTAB-1000. As previously observed by Vural and Sari [43], the DS species could strongly interact with the positive charges of the alumina surface, the surfactant head groups remaining in the structure at high temperatures.

Weak peaks at 31.68, 45.4 and 56.44° (2θ) observed for the Fe–AlO-HDA-100 sample seemed to be due to the surfactant. The solid calcined at 500 °C, Fe–AlO-HDA-500, was essentially amorphous, but extremely weak peaks emerged at 22.56, 23.56, 24.80, 25.52, 31.76, and 34.04 (2θ), which can be assigned to magnetite (Fe_3O_4), suggesting the beginning of the formation of a crystalline phase. Fe^{2+} ions might have been formed because of the reductive conditions originated during decomposition of the organic precursor. Concerning sample Fe–AlO-HDA-1000, the sharp peaks due to the α-Al_2O_3 phase were observed,

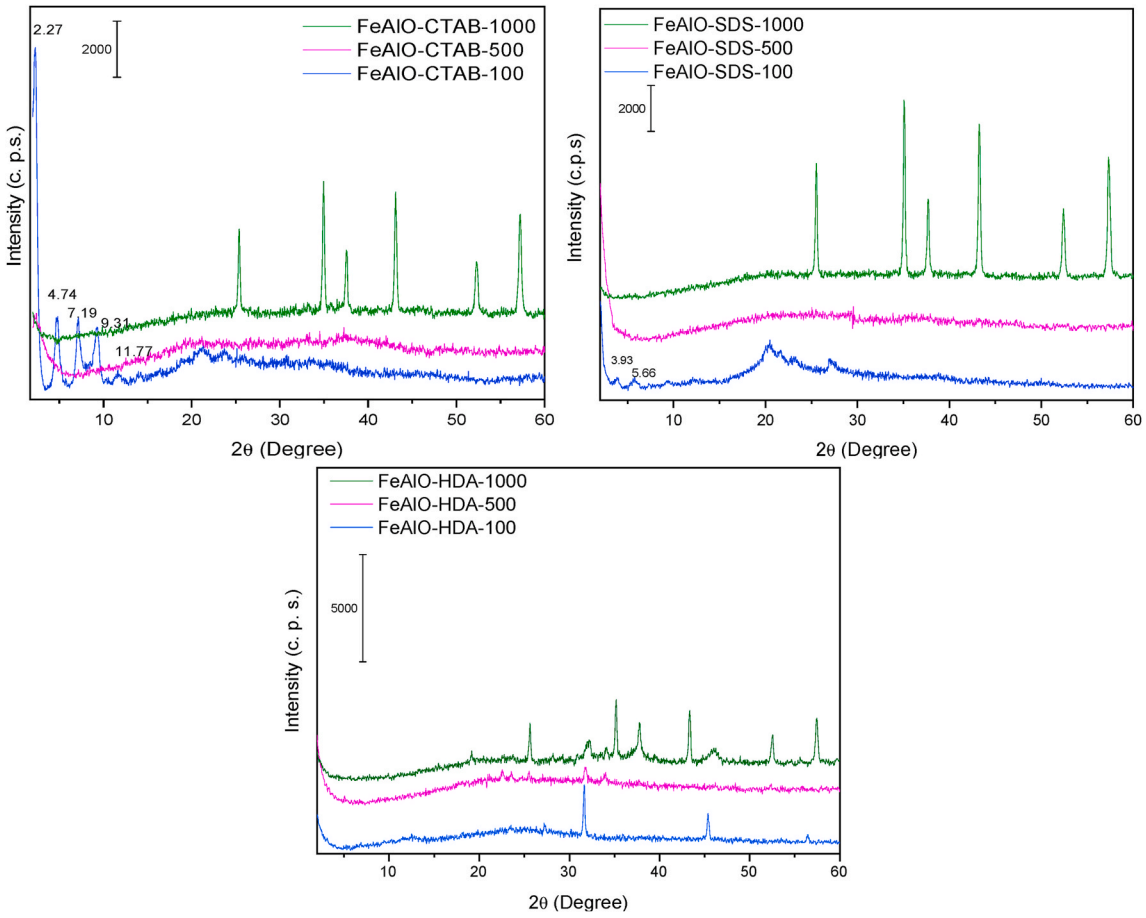

Fig. 1. PXRD diffractograms of the dried and calcined solids obtained from each of the surfactants.

with typical reflections at 25.64, 35.2, 37.76, 43.36, 52.56, and 57.4 (2θ), but they were less intense than for the samples prepared with the other surfactants and calcined at 1000 °C, suggesting a lower crystallinity. This could be attributed to the fact that the neutral surfactant contained amine groups that could interact more effectively with Fe^{3+} ions, resulting in Fe_3O_4 clusters and inducing the presence of iron outside the alumina framework. The weaker peaks at 32.04, 34.08, 37.76, and 45.96° (2θ) were tentatively assigned to a mixture of magnetite and maghemite phases.

The influence of the surfactant was analyzed by comparing the solids calcined at the same temperature (Fig. S2). As indicated, the samples calcined at 500 °C were mainly amorphous, but the development of very small peaks in the PXRD diagrams can be clearly observed for the solid obtained from HAD, denoting the starting steps of the formation of crystalline phases. In the case of the solids calcined at 1000 °C, α-Al_2O_3 was observed in all cases, with the only difference that peaks were more intense in the solid obtained from SDS. In addition, the low intense peaks due to the phases involving iron were clearly observed for the HAD-derived solid.

The thermal curves showed progressive mass losses for all the solids (Fig. 2), but with significant differences depending on the surfactant used during the synthesis. The first mass loss (~15%) for sample FeAlO-CTAB-100 occurred from room temperature to ca. 200 °C, and it was assigned to removal of water and (if any) solvent molecules. Although the solids had been previously dried at 100 °C, mass loss from room temperature was probably due to removal of water adsorbed during handling; indeed, this sample was hygroscopic. During the storage and handling of the as-prepared solid (dried at 100 °C), it acquired moist characteristics, which indicated a strong hydrophilicity, in agreement with the reported thermal effect and with FTIR results (*vide infra*). This behavior has been reported in the literature for samples similar to those here studied; for instance, by the presence of water molecules weakly adsorbed on the surface of CoAl-silicate materials [18], and describing a hygroscopic surface for iron-alumina solids [25]. Two further mass losses were recorded from 200 °C upwards, one up to ca. 250 °C and the second up to 550 °C. In both cases, strong, broad, exothermic effects were recorded, suggesting combustion of the organic components of the solid [19]; indeed, CTAB can be easily removed by combustion [44]. Mass loss was complete at ca. 650 °C. This might correspond to removal of more strongly retained surfactant molecules, and pyrolysis and removal of residual groups, but endothermic dehydroxylation due to condensation of residual hydroxyl groups may also happen. The hydroxyl groups may have been formed by hydrolysis of residual alkoxide groups with water molecules adsorbed after the synthesis of the solids or by non-hydrolytic hydroxylation reactions, catalyzed by the presence of HCl as a byproduct (and in the present case, also by the presence of HBr). This has been previously observed by Mutin and Vioux [33] and suggests a complex reaction mechanism. No further changes were observed above 600 °C. The mass of the final residue was only ca. 22% of the initial mass, confirming the high content of surfactant and water (~78%) in the synthesized solid.

When SDS was used as a surfactant, the first mass loss step was weak, less than 10% of the initial mass sample, indicating that this solid adsorbed a smaller amount of water than the previous sample (visually, this solid was less hygroscopic than FeAlO-CTAB-100). Again two consecutive mass losses in approximately the same temperature ranges (from 200 to 250 and from 250 to 550 °C) were observed. The exothermic effect corresponding to the first mass loss was rather sharp in this case, noticeably sharper than for the former sample, while the second exothermic peak was somewhat broader, but markedly weaker.

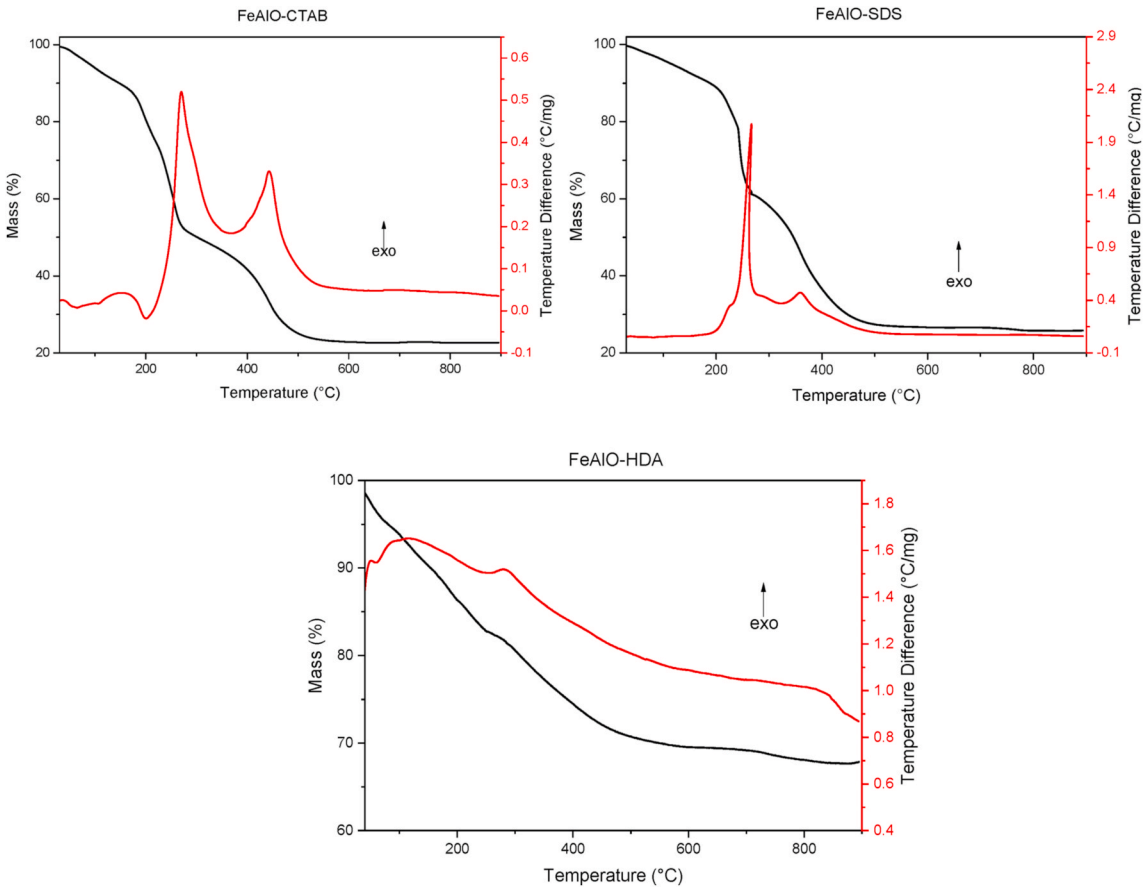

Fig. 2. TG and DTA curves of the solids dried at 100 °C from the three series considered.

The total water and surfactant content was again around 78% of the initial mass of the solid. In other words, these two samples behave in a similar way, except for the lower hygroscopic character of the SDS sample and the lower intensity of the second exothermic effect.

Finally, sample FeAlO-HDA-100 showed a different behavior. First, the total mass loss was only ca. 35% of the initial mass, although the mass lost above ca. 500 °C was very small (in agreement with the results observed for the other two samples). Secondly, the mass loss took place in a continuous way, making impossible to define consecutive independent steps. The DTA curve showed a weak endothermic effect at low temperature, probably due to removal of externally adsorbed water molecules, and a single exothermic effect around 260 °C, i. e., in the same temperature range where the first strong exothermic effect was recorded for the former two sample, suggesting a similar origin for the first peak in the three samples.

The solids had similar FT-IR spectra (Fig. S3). Bands around 3400 and 1600 cm^{-1} in the spectra of the samples calcined at 100 °C are characteristic of O–H bond stretching and deformation of water molecules modes, respectively [45], reinforcing the assumption that the solids contained hydroxyl groups, as suggested by the thermal analyses. The three solids dried at 100 °C also showed bands from 2950 to 2850 cm^{-1} and around 1470 cm^{-1}, due to stretching and bending vibrations of the C–H bonds [31] of the surfactants. They were clearly less intense in the case of FeAlO-HDA-100, in agreement with its lower content of organic matter (despite the molar Fe:Al:surfactant was the same for all the samples, these differences were due to their different chemical formula). After treatment at 500 or 1000 °C, these bands disappeared, indicating that the heat-treatment removed the surfactants. However, some not very intense disturbances were detected in the region of 1470 cm^{-1}, which was compatible with the presence of residual carbon [46].

The presence of weak bands in these same wavenumber ranges (3400 and 1600 cm^{-1}) in the spectra of the solids heated at 500 °C was not surprising, because hydroxyl groups can withstand temperatures of up to ~ 600 °C. In addition, water molecules adsorbed during handling of the solids may have contributed to these bands. In the case of sample FeAlO-HDA-100, the intense band around 3400 cm^{-1} could also be attributed to the N–H bond stretching mode [28], because HDA is a primary long-chain amine.

The bands around 3400 and 1600 cm^{-1} were no longer recorded in the FT-IR spectra of the solids treated at 1000 °C, which exhibited essentially identical FT-IR spectra for all samples, with only bands due to M − O vibrational modes below 1000 cm^{-1}. The intense split absorption band centered between 720 and 570 cm^{-1} referred to Al–O vibrations in an octahedral [AlO_6] environment; no bands due to Al–O vibrations in tetrahedral environment [AlO_4] were detected. α-Al_2O_3 consists of Al^{3+} ions in an octahedral environment, so this absorption band suggested that this phase was formed, confirming that the NHSG method with molecular precursors allowed crystallization of this phase at low temperature [47,48]. The intense band at ca. 430 cm^{-1} was also due to [AlO_6] groups (Al–O–Al vibrations), although some authors have ascribed bands between 500 and 400 cm^{-1} to Fe–O related stretching modes [49]. For the solids treated below 1000 °C, typical bands of [AlO_4] groups in amorphous systems were also noted [47,48].

The N_2 adsorption-desorption isotherms, recorded at – 196 °C, of all the solids calcined at 500 °C (Fig. S4, left) can be included in type IV of the IUPAC classification [50], which is typical of mesoporous materials. The curve for sample FeAlO-CTAB-500 showed a type H2 hysteresis loop due to wedged shaped pores, while the curves obtained for samples FeAlO-SDS-500 and FeAlO-HDA-500 were type H3, related to the presence of slit-shaped pores [50]. Hysteresis indicated an homogeneous distribution of the pore diameters, as confirmed by the distribution charts of the average pore diameter (Fig. S5).

These curves indicate the mesoporous character of the solids, with high homogeneity of the pore diameter of the three materials, as the maxima in these curves, Fig. S5 (left), are not excessively broad. The average pore diameters of solids FeAlO-CTAB-500, FeAlO-SDS-500, and FeAlO-HDA-500 were 90, 50, and 82 Å, respectively, all of them in the mesoporous range [44]. After the heating treatment at 1000 °C the changes in the values of pore size diameter to 205, 213 and 202–373 Å were ascribed to the collapse of the pores, and to crystallization. As it will be shown below, the catalytic activity and specially the selectivity were drastically influenced by the pore size distribution and the specific surface area.

As expected, the use of surfactants during the syntheses yielded materials with relatively large specific surface areas, Table 1. The smallest values were measured for the sample prepared using HDA, probably because it bears the least bulky functional group and is neutral. However, it is important to remember that the PXRD studies confirmed the presence of iron-containing clusters in sample Fe–AlO-HDA-500.

On calcination at 1000 °C the specific surface areas of the samples prepared with CTAB and SDS were drastically reduced to 6 and 5%, respectively, of the values measured for the samples calcined at 500 °C. Such a decrease was much less evident (only 8%) for the sample prepared using HAD. This decrease was undoubtedly related to crystallization of alumina, as concluded from the PXRD analysis of the samples calcined at 1000 °C, yielding to sharp, intense peaks (indicating large crystallites) for the first two samples, while for the HDA-derived sample the peaks remain markedly less intense. Such a crystallization process produced a sintering of the samples, a decrease of the specific surface area and a marked increase in the pore diameter (Fig. S5). Heat-treatment at 1000 °C also gave rise to a much broader pore diameter distribution for all the materials.

In any case, it was rather surprising that, despite the small decrease in its specific surface area upon calcination at 1000 °C, the pore volume of the HDA-derived sample was twice for the sample calcined at 1000 °C than for that calcined at 500 °C. We can tentatively assume that this sample, even after calcination at 500 °C, had retained a significant amount of surfactant within its pores, making them unavailable to the N_2 molecules during the adsorption process, thus accounting for its specific surface area being much lower than those for the other two samples. Upon calcination at 1000 °C these molecules were removed (the TG curve for this sample showed a significant mass loss above 500 °C) and the pores were made available to the N_2 molecules.

Considering the surfactants as the agents that will originate the porous structure in alumina, no large differences should be expected in the pore size when comparing the CTAB and HAD-derived solids, since these surfactants have the same carbon chain length differing only by the polar part, while SDS, slightly smaller in size, should originate smaller pores. This prevision agreed with the experimental data. When comparing the materials treated at 500 and 1000 °C, both the surface area and the pore size changed, since at 1000 °C the solid structure organized itself generating the crystalline structure observed in the PXRD and the elimination of the surfactants that generated an increase in the pore diameter. As highlighted before, the material prepared from HDA had different behavior than those from SDS and CTAB when increasing the calcination temperature from 500 to 1000 °C, mainly by its less intense crystalline character observed by PXRD and the lower collapse suggested by the TEM study (see below), which caused a different behavior of the textural properties. Thus, the pore size of the solids calcined at 500 °C matched with the size of the surfactants, while the pore size at 1000 °C seemed to be independent of the surfactant nature, being a characteristic of the alumina itself. The ratio between the specific surface area and the pore volume was similar for the three solids calcined at 1000 °C, suggesting similar materials in terms of textural properties.

Table 1
Textural properties of iron aluminates.

Sample	Specific surface area (m^2/g)	Pore volume (cm^3/g)	Average pore diameter (Å)	Reference
Al_2O_3	309	–	–	[22]
α–alumina	5.8–11.6	–	–	[43]
FeAlO-CTAB-500	284	0.77	90	This work
FeAlO-SDS-500	151	0.31	50	This work
FeAlO-HDA-500	65	0.19	82	This work
FeAlO-CTAB-1000	17	0.09	205	This work
FeAlO-SDS-1000	7	0.04	213	This work
FeAlO-HDA-1000	60	0.39	202–373	This work

It should be remarked here that a reference solid was prepared under the same conditions, but without using any surfactant, in order to use it as blank for the catalytic tests. However, this solid showed a practically negligible specific surface area and its use was ruled out. On the other hand, alumina prepared by NHSG showed a specific surface area of 309 m^2/g [22]. Vural and Sari [43] used the surfactant strategy for generation of mesoporosity in the alumina matrix, and the values of specific surface area of the heat-treated solids ranged between 5.8 and 11.6 m^2/g. These authors showed that the incomplete removal of the surfactants could induce the decrease of the specific surface area, due to the collapse of the alumina framework.

The transmission electron micrographs of sample FeAlO-CTAB-100 (Fig. 3), which contained stacked surfactant molecules as suggested by the PXRD results, indicated a sort of wormhole-like mesoporous structure (Fig. 3b and c) [51]. Aguado et al. [52] reported this type of structure when they characterized different γ-alumina samples prepared by the traditional (hydrolytic) sol–gel method in the presence of CTAB; the difference in our case was that such a structure was obtained after controlled heat-treatment of the prepared solid. An interesting structure was observed for sample FeAlO-CTAB-500 (Fig. 3d and e), which consisted of "fibers", or nanowires, entangled on the surface of bulky particle clusters. This could explain the relatively large specific surface area of this material, 284 m^2/g. It is noteworthy that heat-treatment at 1000 °C caused the fibrous structure to arrange into bulky and dense agglomerates, which would effectively account for the sharp decrease in the specific surface area.

The micrographs for the other samples are included in the Supplementary Material section. The micrographs for sample FeAlO-SDS-100 (Figs. S6a and S6b) showed "dark" agglomerates on its surface, which seemed to be rough/porous; however, its structure was not organized, which confirmed the PXRD results. After heat-treatment at 500 °C, DS was removed (FeAlO-SDS-500, Figs. S6c and S6d). This was consistent with the textural properties, as FeAlO-SDS-500 had a relatively large specific surface area and average pore diameter (151 m^2/g and 50 Å, respectively). Furthermore, heat-treatment at 1000 °C (Figs. S6e and S6f) afforded a solid whose micrograph profile resembled that of FeAlO-CTAB-1000; that is, the particles were aggregated, forming dense clusters, a conclusion in agreement with the textural parameters measured for the 1000 °C calcined sample.

Sample FeAlO-HDA-100 contained mainly agglomerates in the form of rods, as well as some (not perfect) spherical particles (Figs. S7a and S7b). Lighter regions – surfaces of the agglomerates – were also detected, which pointed to the porous character of the material. The presence of rod-shaped agglomerates was even more noticeable for sample FeAlO-HDA-500 (Fig. S7c). Interestingly, Figs. S7d and S7e suggested that the rods probably originated from the combination of several nanorods or "nanowires". Thus, HDA removal by treatment at 500 °C did not cause the structure to collapse, and a relative organization was retained after this heat-treatment. Concerning sample FeAlO-HDA-1000 (Figs. S7f and S7g), the images revealed a very different profile as compared to the other samples calcined at 1000 °C, FeAlO-CTAB-1000 and FeAlO-SDS-

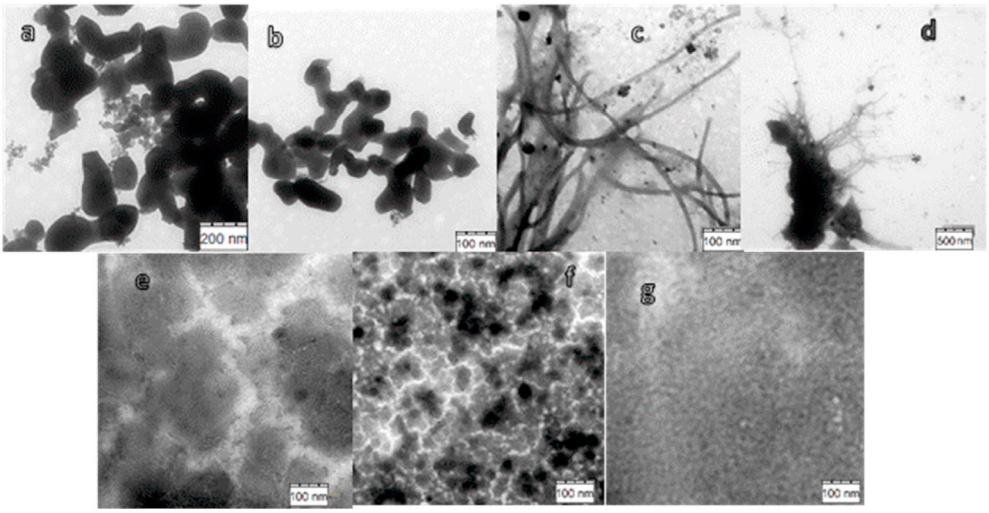

Fig. 3. TEM images of samples FeAlO-CTAB-100 (a, b, and c), FeAlO-CTAB-500 (d and e), and FeAlO-CTAB-1000 (f and g).

1000. Some of the rods in sample FeAlO-HDA-1000 collapsed, but some of them were still observable after heat-treatment. High temperature heat-treatment is known to favor particle aggregation, generating dense agglomerates [53].

Remarkably, the structure of sample FeAlO-HDA changed only slightly when the material was heated at 1000 °C (if compared to that of the material calcined at 500 °C), which was in line with the small decrease in the specific surface area measured for this solid with respect to that of sample FeAlO-HDA-500 (60 and 65 m^2/g, respectively). This characteristic could account for sample FeAlO-HDA-1000 showing different catalytic properties than samples FeAlO-CTAB-1000 and FeAlO-SDS-1000.

The SEM micrographs (Figs. S8–S10) indicated that the type of surfactant and the heat-treatment temperature did not markedly influence

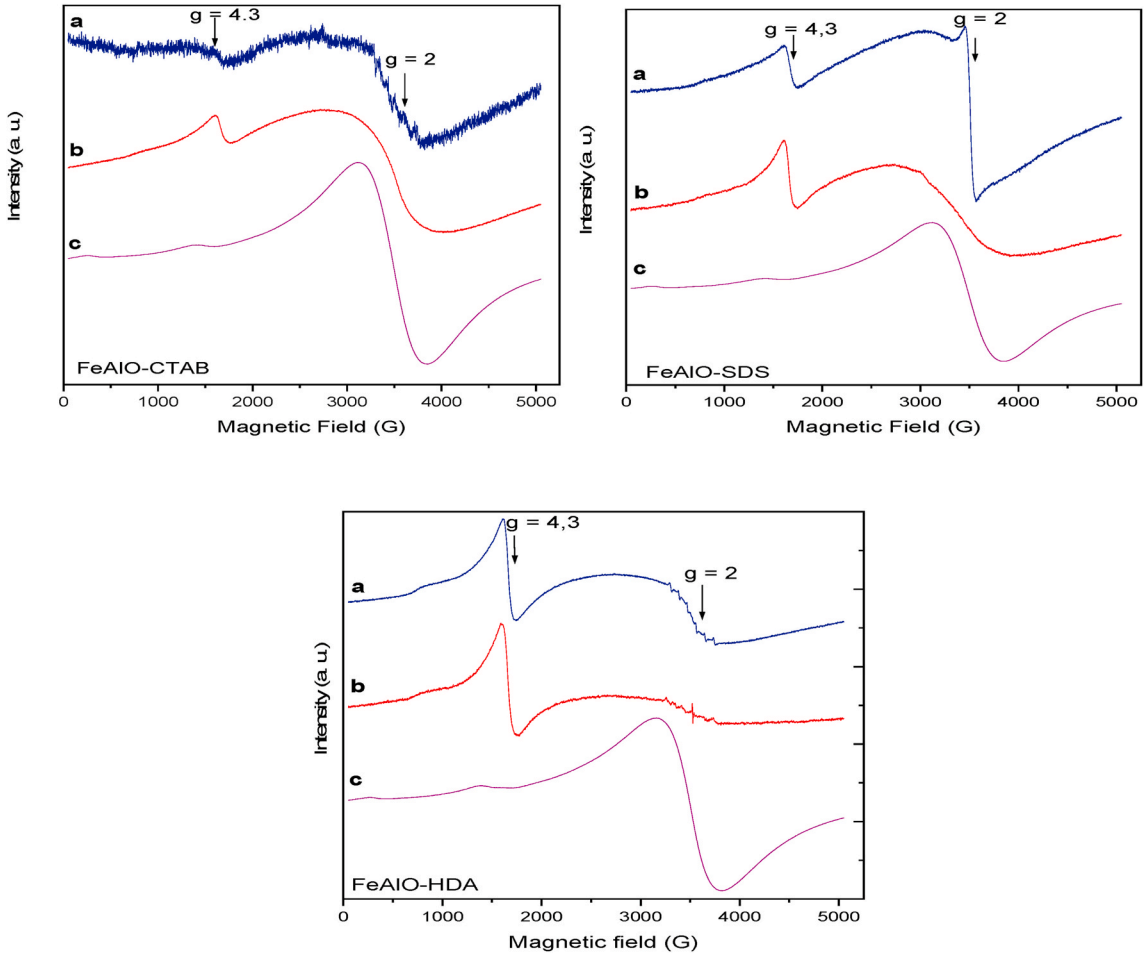

Fig. 4. EPR spectra of the different samples. In each case, a: solid dried at 100 °C, b: solid calcined at 500 °C, and c: solid calcined at 1000 °C.

the surface morphology of the solids at the micrometric level. Likewise, Rinaldi and Schuchardt [54] did not observe any effect of the heat-treatment temperature when they prepared aluminas by the hydrolytic sol–gel method. In our case, the SEM images showed particles with relatively porous/rough surfaces even for the solids heated at 1000 °C.

The main expected elements —iron, aluminum, and oxygen— were present on the surface of all the solids (Figs. S8–S10). Iron mapping indicated that the iron surface concentration increased with the calcination temperature, and that iron was homogeneously distributed on the surface of the solids. Such an increase may have simply resulted from the removal of organic species and residual groups, thereby increasing the relative concentration of permanent, not removable, inorganic elements; or even from the decrease in the specific surface area. Alternatively, iron ions in the matrix structure may have migrated to the surface upon increasing calcination temperature, forming iron oxide clusters [20]. If this was the case, iron oxide clusters were very small and could not be detected by PXRD, except in sample Fe–AlO-HDA-1000, see Fig. 1.

The homogeneous distribution of the elements on the surface of the solids is worth highlighting. Although sol–gel processes (hydrolytic and non-hydrolytic routes) frequently favor formation of homogeneous materials [11,55], the surfactants could chelate Fe^{3+} or Al^{3+} ions (mainly DS, which is anionic, and HDA, neutral, but bearing an amine group), resulting in phase segregation. The absence of this phenomenon proved the successful use of surfactants in the NHSG process.

Fig. 4 includes the EPR spectra of the solids from the three series of samples. All the spectra displayed signals at g = 4.3 and g = 2, with different signal intensities. The signal close to g = 2 was assigned to a strong interaction between high spin Fe(III) ions in octahedral positions of the lattice and the bulk material. Its intensity roughly increased with the calcination temperature, indicating an increase in the symmetry of the sites occupied by the iron ions. The signal close to g = 4.3 corresponds either to strongly distorted orthorhombic sites located on the surface of the particles, to isolated Fe(III) ions dispersed in the solid matrix [28], or to strongly rhombic distorted species in tetrahedral or octahedral environments [22,28,44].

The signal at g = 4.3 was attributed to Fe^{3+} ions in a rhombic environment [25]. This signal has also been reported in systems involving heterogenized metalloporphyrins on inorganic supports [22,48,56]. In addition, all the solids heated at 100 °C and sample Fe–AlO-HDA-500 revealed a low-intensity signal of six lines around g = 2, ascribed to the presence of manganese (II) or manganese (IV) ions, probably as a small amount of impurity.

The three solids calcined at 1000 °C showed similar spectra, with an almost undetectable signal at g = 4.3 and a high-intensity, well-defined one at g = 2. The predominance of the latter signal in the spectra could be related to the high crystallinity of these solids and suggested isomorphic substitution of Al^{3+} for Fe^{3+} ions in the octahedral [AlO_6] groups, as already discussed. The signal was considerably symmetrical. Nevertheless, formation of iron oxide aggregates on the surface of the solids cannot be ruled out given that such aggregates also generate intense signals at g = 2 [57], and that chemical mapping by EDS demonstrated increased concentration of iron on the surface of the solids with increasing the heat-treatment temperature. In any case, there were evidence that Fe^{3+} ions were strongly linked to the polymeric networks of the solids, which was interesting for heterogeneous catalysis given that metal ions poorly adsorbed to supports can easily leach from the matrix during catalytic reactions.

The electronic spectra of the samples calcined at 500 and 1000 °C for the CTAB series samples are included in Fig. 5, while those for the other two series are included in Fig. S11. The electronic spectrum of FeAlO-CTAB-500 (Fig. 5) displayed a broad band between 400 and 250 nm, with shoulders at 470 and 229 nm, while the spectrum of sample FeAlO-CTAB-1000 (Fig. 5) showed more defined bands and shoulders at 458, 383, 335, 262, and 220 nm. The spectra of FeAlO-CTAB and FeAlO-SDS solids (Fig. S11) were similar.

In all cases, an intense absorption was observed at low wavelength, progressively decreasing its intensity as the wavelength is increased. On comparing all six spectra, it can be observed that the absorption band sharpened when the calcination temperature was increased from 500 to 1000 °C.

The higher-energy bands, from 200 to 250 nm, were characteristic of metal-ligand charge transfer (MLCT) processes [58]. These charge transfer bands can also be attributed to dπ-pπ transitions between iron and oxygen ions, in tetrahedral [FeO_4] [58,59] or octahedral [FeO_6] [58] systems, in the polymeric matrix (Fe–O–Al bonds) [60] (or even involving residual OH groups), which would be a strong indication that Fe^{3+} ions were not simply adsorbed on the supports. Both situations could occur; however, on the basis of the EPR signal at g = 4.3 characteristic of iron ions with distorted geometry in a rhombic environment, Fe^{3+} ions must have been incorporated into the alumina matrix.

All the other UV–Vis bands of the materials were typical of originally forbidden *d-d* transitions, probably allowed because of structural distortions. The spectra of all the synthesized solids displayed bands at approximately 460, 540, and 690 nm. After comparison with other techniques, Bordiga et al. [58] assigned *d-d* transition bands at 357, 392, 417, 455, and 526 nm to isolated Fe^{3+} ions with tetrahedral geometry. In turn, Jitianu et al. [49] attributed the bands at 430–460, 545, and 650 nm to Fe^{3+} ions supported in the polymeric network, but in an octahedral geometry. Therefore, UV–Vis absorption spectroscopy cannot distinguish between tetrahedral and octahedral geometry. Concerning the systems reported here, the EPR results showed Fe^{3+} ions in rhombic environment, whereas the IR spectroscopy revealed Al^{3+} ions in octahedral environment, characteristic of the α-Al_2O_3 phase (verified by PXRD). Therefore, Fe^{3+} ions should be located in different sites with different geometries. In other words, the materials contained Fe^{3+} ions isolated in tetrahedral environment, Fe^{3+} ions isolated in octahedral environment (in the case of the materials heat-treated at 1000 °C), and iron oxide (Fe_2O_3) clusters (in the case of the heat-treated materials). At

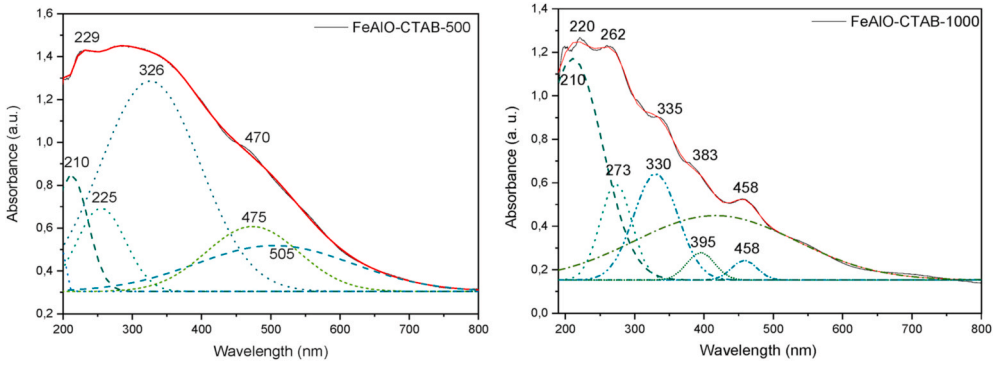

Fig. 5. Electronic spectra (original and with deconvolution) of FeAlO-CTAB materials.

this point, the presence of Fe^{2+} ions cannot be ruled out. It should be noticed that the overall broadness of the complex absorption band slightly decreased when the calcination temperature was increased from 50 to 1000 °C, suggesting that calcination at high temperature leads to more symmetric environments for the Fe(III) ions, so decreasing the chances for forbidden *d-d* transitions.

Table 2 shows results on the Brønsted acidity of the samples, determined by the cyclohexylamine method; the mass considered for each solid was the mass that was calculated to exist at 200 °C according to the TG curves. At this temperature, adsorbed water, residual solvent molecules, byproducts, and poorly adsorbed cyclohexylamine molecules had already been removed from the solids.

A significant acidity was observed for the solids calcined at 500 °C, whereas acidity was practically zero for the solids calcined at 1000 °C if the values were referred to mass unit. These results resembled those reported by Ricci et al. for iron (III) alumina materials [25]. However, acidity being a surface property, it is worthwhile to also refer the values per surface area unit. The values thus calculated are also included in Table 2. As it can be seen, the decrease was only ca. 12% for sample FeAlO-DTBA on calcining at 1000 °C (compared to the value calculated for the sample calcined at 500 °C), and ca. 40% for sample Fe–AlO-SDS, but 90% for sample FeAlO-HDA. For materials based on alumina, the main source of Brønsted acidity is the presence of Al–OH groups on the surface of the particles. Previous results of thermal analysis and FT–IR spectroscopy results had shown the presence of these groups in alumina-based solids.

After heat-treatment at 1000 °C, the hydroxyl groups must have condensed (dehydroxylation), which would explain the extremely low Brønsted acidity of the samples calcined at this temperature. In addition, the low specific surface area would have given rise to a decrease in the absolute number of acid sites, but its surface concentration did not decrease as much.

3.2. Cyclooctene epoxidation

The first catalytic reaction studied was the oxidation of cyclooctene with H_2O_2, as this substrate generally affords cyclooctene oxide, a relatively stable epoxide, as the main product. For this reason, cyclooctene is commonly used as a "diagnostic substrate" to determine the catalytic activity, to establish the ideal reaction conditions, and to elucidate reaction mechanisms [18,28].

Fig. 6 shows the conversion results (mol of product/initial mol of substrate, in %) of the preliminary tests carried out with all the solids calcined at 500 and 1000 °C. A higher H_2O_2 concentration (Fe^{3+}/H_2O_2/substrate molar ratio of 1:100:500) provided better conversion results; that is, favored larger cyclooctene conversion, as previously observed for other iron-alumina catalysts [25]. To improve these results, cyclooctene epoxidation tests were conducted with anhydrous H_2O_2 instead of aqueous H_2O_2 (data also in Fig. 6).

For each pair of samples, that calcined at 500 °C showed a lower catalytic activity than that calcined at 1000 °C. This behavior might be due to the larger concentration of Brønsted acid sites in the 500 °C-calcined samples. However, there is no linear relationship between the concentration of acid sites and the catalytic activity, suggesting the presence of acid sites acting in different manners. Rinaldi et al. [61] reported the presence of different types of acid sites in alumina: those denoted as types Ia and Ib by these authors were weak, and those denoted as types IIa, IIb, and III were strong and could act as proton donors; the former sites were the active centers for product formation, whilst the latter sites accounted for non-productive H_2O_2 decomposition, which justified the low catalytic yields.

When using hydrated H_2O_2 and the samples calcined at 500 °C, the worst results were observed for sample FeAlO-CTAB-500. The solids calcined at 1000 °C showed higher catalytic activity, despite their low concentration of acid sites and lower specific surface area. Sample FeAlO-SDS-1000 (34% conversion) was far better than the other samples; this material showed the lowest specific surface area (7 m^2/g), but the highest surface concentration of acid sites among the 1000 °C-calcined samples, and its higher conversion suggested a lower ability for H_2O_2 decomposition. In other words, both textural characteristics and acid sites influenced the catalytic systems; the presence of acid sites on the surface of the solids seemed to affect the catalytic results by inducing H_2O_2 disproportionation and not resulting in heterolytic cleavage, which is interesting for cyclooctene conversion. Because the oxidant was used in excess, the reaction medium contained a significant amount of water, which made difficult the access of the hydrophobic substrate to the active catalyst sites, as already noted by Rinaldi et al. [62].

The use of anhydrous H_2O_2 significantly increased cyclooctene conversion. For the solids calcined at 1000 °C, substrate conversion was at least 55%, whereas the best result achieved for aqueous H_2O_2 was 34%. The solids calcined at 1000 °C again showed, using the anhydrous oxidant, better catalytic activity than those calcined at 500 °C, again suggesting that the acid sites existing in the solids heated at 500 °C deactivated H_2O_2. Substitution of water for ethyl acetate, which is much less hydrophilic, facilitated the access of the substrate to the catalysts surface, improving the catalytic activity. The liquid phase of the catalytic systems proved to be more homogeneous in the presence of anhydrous H_2O_2 than aqueous H_2O_2 (visual observation).

Hydrogen peroxide disproportionation was analyzed after 24 h reaction (Table 3). Considering that the amount of H_2O_2 was five times greater (in mol) than the amount of substrate, only a small fraction of H_2O_2 was used to produce cyclooctene oxide, whereas the amount of non-productively deactivated H_2O_2 was extremely high, 80–92% for all the solids, except for FeAlO-HDA-1000; it was always higher for the solids calcined at 500 °C than for the corresponding one calcined at 1000 °C. In the case of FeAlO-HDA-1000, H_2O_2 decomposition was smaller, and the catalytic activity was higher. This result evidenced that Brønsted sites (which concentration was larger for samples calcined at 500 °C than for those calcined at 1000 °C) and the specific surface area influenced drastically the catalytic results; these Brønsted acid sites were responsible for non-productive H_2O_2 decomposition, in agreement with previously discussed results on quantification of acid sites by cyclohexylamine.

As sample FeAlO-HDA-1000 showed the highest catalytic conversion when using anhydrous H_2O_2, it was selected to insight in the nature of the possible reactive intermediate species, by carrying out the reaction in the presence of hydroquinone, a known radical scavenger in catalytic tests [37,38]. This approach was adopted by considering the large discussion in the literature on whether the reactive intermediate species in this type of reactions is or is not a radical one [63,64], which may be related to the Fenton process, involving formation of highly reactive and non-selective hydroxyl radicals ($OH^{\bullet}$). Cyclooctene conversion was essentially the same, which pointed out to a non-radical mechanism. Thus, the reaction may have occurred via the other mechanism proposed for hydrocarbon oxidation under mild conditions, which is considerably selective. This mechanism involves high-valence iron ions as active species, namely, ferryl or perferryl ions (Fe^{IV}=O and Fe^{V}=O, respectively), which have also been observed for biological systems such as cytochromes P-450 and synthetic porphyrins [65–67]. The route proposed for the formation of perferryl intermediate is: $Fe^{III} + H_2O_2 \rightarrow$

Table 2
Brønsted acidity of heat-treated iron-alumina samples.

Catalyst	Acidity/mmol H^+/g^{-1}[a]	Acidity/sites·nm^{-2}
FeAlO-CTAB-500	0.57	1.20
FeAlO-SDS-500	0.75	2.98
FeAlO-HDA-500	0.47	4.34
FeAlO-CTAB-1000	0.03	1.06
FeAlO-SDS-1000	0.02	1.71
FeAlO-HDA-1000	0.04	0.40

[a] for each mmol of desorbed cyclohexylamine, 1 mmol of H^+(a Brønsted acid site) was considered. Referred to mass of the solid at 200 °C.

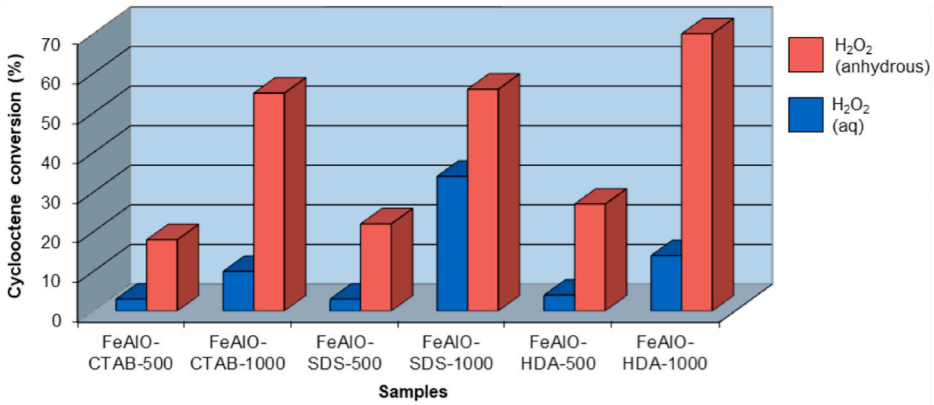

Fig. 6. Results of cyclooctene epoxidation tests after reaction for 24 h in the presence of iron-alumina using aqueous (70 wt%) or anhydrous (42 wt% in ethyl acetate) H_2O_2 as oxidant. Conditions: Fe^{3+}/H_2O_2/substrate molar ratio = 1:100:500; T = 50–55 °C.

Table 3
Amount of H_2O_2 used for cyclooctene oxide production and non-productively decomposed H_2O_2 after cyclooctene epoxidation with anhydrous H_2O_2 (reaction time 24 h).

Catalyst	Production of cyclooctenoxide (%)	Non-productive decomposition (%)
FeAlO-CTAB-500	3	92
FeAlO-CTAB-1000	10	80
FeAlO-SDS-500	4	91
FeAlO-SDS-1000	10	83
FeAlO-HDA-500	5	90
FeAlO-HDA-1000	13	10

Fe^{III}–O–OH → Fe^{V}=O + OH^-. According to Nunes et al. [67] and Arends and Sheldon [68], in a non-radical catalytic reaction, both Fe^{III}–O–OH (iron-peroxo) and Fe^{V}=O (iron-oxo) species can transfer oxygen to the substrate (metal-peroxo and metal-oxo mechanisms, respectively) as previously discussed in the literature [18,28].

Concerning reuse, none of the catalysts showed a significant decrease in its catalytic activity after the three recycling cycles considered (Table 4); even cyclooctene conversion increased. As indicated before, calcination at 500 °C, and mainly at 1000 °C, stabilized the active phase by making the catalysts truly heterogeneous. However, under the conditions here used in the tests, especially high H_2O_2 concentration and the presence of water, the catalyst leached from the active phase to the solution, and more active sites probably became better available in the materials due to small textural changes.

Table 4
Recycling tests for cyclooctene epoxidation, after 24 h reaction (Fe/cyclooctene/H_2O_2 molar ratio = 1:100:500; T = 50–55 °C) using anhydrous H_2O_2.

	Cyclooctene conversion (%)			
Catalyst	Test	1st reuse	2nd reuse	3rd reuse
FeAlO-CTAB-500	18	16	22	34
FeAlO-CTAB-1000	55	60	100	90
FeAlO-SDS-500	22	25	20	25
FeAlO-SDS-1000	56	54	67	92
FeAlO-HDA-500	27	21	30	40
FeAlO-HDA-1000	70	80	78	80

3.3. Cyclohexane oxidation

All the solids prepared herein catalyzed cyclohexane oxidation (Fig. 7), providing promising results, especially when compared to the industrial process [69–71]. The samples calcined at 500 °C were markedly less active than those calcined at 1000 °C, although the values for sample FeAlO-HDA-1000 were rather low. Catalyst FeAlO-CTAB-1000 exhibited the greatest total cyclohexane conversion, 25%, after 48 h reaction, but selectivity was small (cyclohexanone/cyclohexanol molar ratio 1.1:1). Independently of iron (III) location on tetrahedral or octahedral sites (discussed in the UV–Vis and EPR sections), selectivity was very low, as previously reported by Ricci et al. [25] and Mikhalyova et al. [72]. A new efficient iron catalyst for olefin epoxidation with hydrogen peroxide has confirmed that selectivity depends on different factors, such as acidity, porosity, and polarity [72]. Cyclohexanone can be formed directly from cyclohexane or from further oxidation of cyclohexanol previously produced from cyclohexane (overoxidation). To evaluate cyclohexanone production, a test was carried out by using cyclohexanol as substrate under the same conditions. Cyclohexanol conversion to cyclohexanone was 20%, which indicated that at least a portion of the cyclohexanone formed in the cyclohexane oxidation tests stemmed from cyclohexanol overoxidation, as reported by other authors [18,73].

Shul'pin [42] found that cyclohexylhydroperoxide (CHHP) can be produced in this reaction along with cyclohexanol and cyclohexanone. In most cases, CHHP is not detected because it decomposes into cyclohexanol and cyclohexanone when the mixture of the reaction products is injected into the chromatograph. Consequently, if CHHP is formed, the alcohol and ketone concentrations determined by GC are not necessarily the real ones formed during the catalytic reaction. To elucidate if CHHP is formed in our case, after analysis by GC of the reaction catalyzed by FeAlO-CTAB-1000, triphenylphosphine (PPh_3) was added to the reaction medium, which composition was analyzed again after 20 min. PPh_3 is a strong reducing agent and therefore reduces CHHP (if formed) to cyclohexanol; so, if CHHP was present in the reaction medium, addition of PPh_3 should increase the cyclohexanol concentration, while the cyclohexanone concentration should remain the same [39]. The results of this test (Table 5) showed that although the amount of cyclohexanone slightly decreased, the amount of cyclohexanol clearly increased, showing that it actually corresponded to the sum of previous existing cyclohexanol and CHHP, demonstrating that CHHP was formed during the catalytic tests, as reported, for example, for Fe-complexes functionalized kaolinite [73]. The presence of CHHP as a byproduct of cyclohexane oxidation strongly supported a non-radical peroxo route mechanism (or, at least, it was proven that this mechanism existed).

TON and TOF values for the alumina catalysts are shown in Table 6. These values were remarkably similar before and after heating

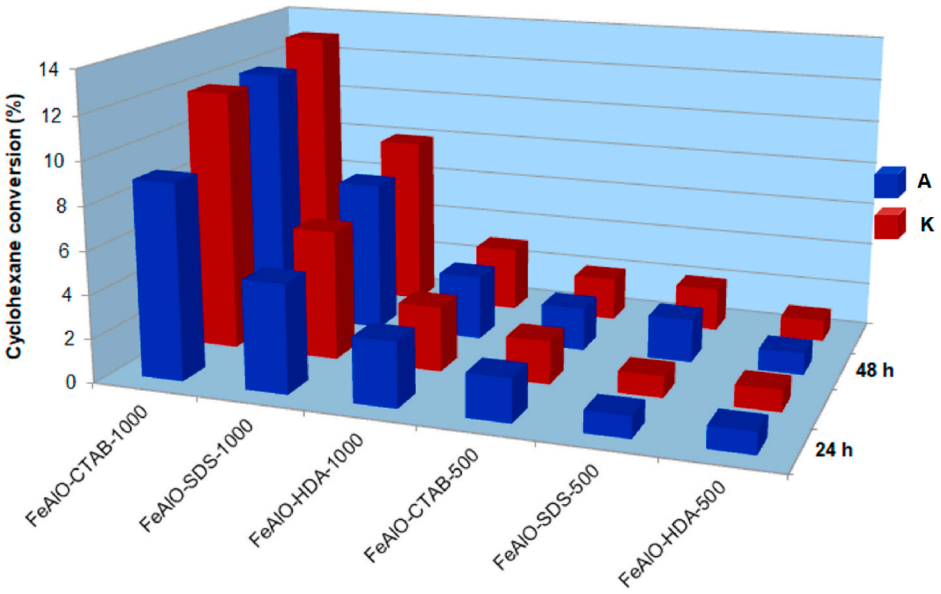

Fig. 7. Catalytic results for iron aluminates during cyclohexane oxidation by anhydrous H_2O_2 (42 wt% ethyl acetate) as oxidant. Conditions: Fe^{3+}/H_2O_2/substrate molar ratio = 1: 100: 500; T = 50–55 °C (A = alcohol (cyclohexanol); K = ketone (cyclohexanone)).

Table 5
Cyclohexane conversion after oxidation reaction for 48 h catalyzed by FeAlO-CTAB-1000 (Fe^{3+}/H_2O_2/substrate molar ratio = 1:100:500; T = 50–55 °C), and conversion after addition of PPh_3 (analyzed 20 min later).

Test	Cyclohexanol (%)	Cyclohexanone (%)
Without PPh_3	12	13
With PPh_3	17	10

Table 6
TON and TOF values in the oxidation of cyclooctene after 24 h of reaction and cyclohexane after 48 h of reaction, respectively.

	Cyclooctene		Cyclohexane	
Catalyst	TON	TOF (h^{-1})	TON	TOF (h^{-1})
FeAlO-CTAB-500	16	0.67	3	0.06
FeAlO-CTAB-1000	22	0.92	10	0.21
FeAlO-SDS-500	27	1.13	5	0.10
FeAlO-SDS-1000	23	0.96	6	0.12
FeAlO-HDA-500	43	1.79	2	0.04
FeAlO-HDA-1000	55	2.29	4	0.08

Turnover number (TON) = amount of products conversion (mol)/amount of iron (III) (mol) and Turnover Frequency (TOF) = TON/time of reaction.

treatment of the catalysts at 500 and 1000 °C. Whichever the type of surfactant used, a small increase was observed after calcination of the solids based on CTAB and HDA surfactants, confirming that calcination induced the generation of active sites on the surface of the catalysts, as indicated by the determination of the acid sites. Considering the TON and TOF values, calcination at 1000 °C led to a low improvement and, from the energetic consumption point of view, it may not be industrially justified, as with some adjustments of the system and reaction medium the catalysts calcined at 500 °C may achieve the same conversions.

3.4. *n*-Hexane oxidation

n-Hexane oxidation can afford adipic acid, a monomer used in the production of nylon-6,6. However, this reaction depends on catalyst selectivity even more than on cyclohexane oxidation, and oxidation of primary and secondary carbons is very difficult [74]. To date, good academic results have been obtained by Raja and Thomas [75]: about 10% *n*-hexane conversion with about 30% selectivity for adipic acid after 24 h of reaction in the presence of cobalt aluminum phosphate as catalyst, oxygen as oxidant, pressure of ca. 15 atm, and a temperature of 100 °C. In addition, *n*-hexane oxidation can provide eight main products, namely, hexanal, hexan-2-one, hexan-3-one, hexan-1-ol, hexan-2-ol, hexan-3-ol, hexanoic acid, and hexanedioic acid (adipic acid).

In the present work, all the materials catalyzed the oxidation of about 7% of *n*-hexane to hexanoic acid, hexan-1-ol, hexan-2-ol, hexan-3-ol, hexan-2-one and hexanal (these two ones determined together), and hexan-3-one (Fig. 8). The behavior of the solids resembled the behavior verified in the cyclohexane oxidation tests; the solids calcined at 1000 °C showed greater catalytic activity than the solids calcined at 500 °C.

As observed, hexan-3-one was obtained with a great selectivity. Although position 3 of the chain in hexane is the easiest one to be oxidized, the selectivity for this product deserved attention, especially in the case of the samples derived from FeAlO-HDA, which provided 100% selectivity. The high selectivity of these solids could be attributed to their morphologies and specific surface areas, which underwent few changes upon increasing the calcination temperature from 500 to 1000 °C.

3.5. *Homogeneous oxidation*

The oxidation of the three substrates was also carried out under homogeneous conditions, by using iron chloride (in the amount equivalent to the Fe content in the solid samples) and the same reaction conditions. In the case of cyclooctene epoxidation, the yield obtained was ~2%, whereas the catalyst was not active for cyclohexane and *n*-hexane oxidation. Hence, the alumina matrix played a crucial role in promoting the efficiency and selectivity of the materials by applying the principle of the isolated site of biological systems, as recently proposed for polymeric matrixes that can control the access of the substrate to the catalyst active sites [18]. Sample FeAlO-HDA-1000 clearly mimicked the site isolation principle and directed the hydrocarbon for oxidation, giving higher selectivity for hexan-3-one (see Fig. 9).

4. Conclusions

Mesoporous Fe(III)-alumina materials were efficiently prepared by the non-hydrolytic sol–gel method. The use of surfactants (cetyltrimethylammonium bromide, sodium dodecylsulfate, or

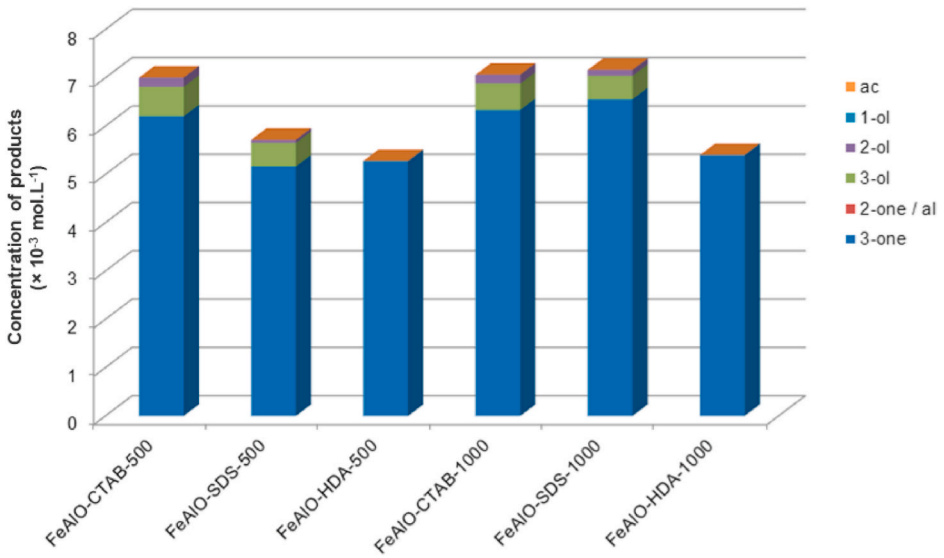

Fig. 8. Catalytic oxidation of *n*-hexane with iron aluminates for 24 h. Molar ratio: Fe:n-hexane/H_2O_2 = 1:100:500, T = 50–55 °C (ac: hexanoic acid; 1-ol: hexan-1-ol; 2-ol: hexan-2-ol; 3-ol: hexan-3-ol; 2-one/al: hexan-2-one and hexanal (determined together); 3-one: hexan-3-one).

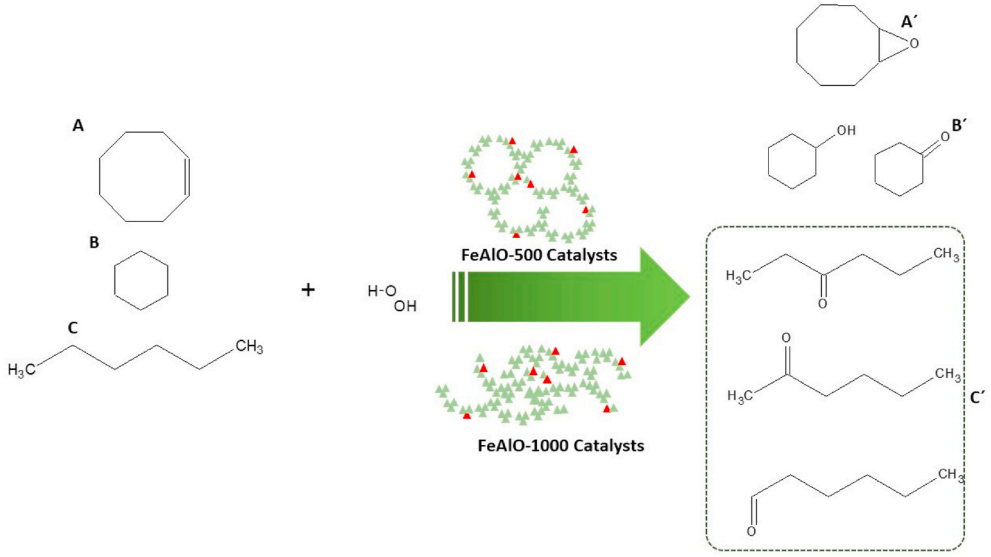

Fig. 9. Schematic representation of oxidation reactions catalyzed by Fe–AlO catalysts.

hexadecylamine) increased the specific surface area of all the materials, mainly cetyltrimethylammonium bromide. Fe(III) was incorporated into the alumina matrix and showed an homogeneous dispersion. The catalytic activity of the solids resulted from a complex combination between acid sites and specific surface area. For cyclooctene oxidation, the solids calcined at 1000 °C, with lower concentration of acid sites, showed better catalytic activities, mainly when the surfactant used during synthesis was sodium dodecylsulfate (34% conversion). As for cyclohexane oxidation, the solid obtained from cetyltrimethylammonium converted 25% of the substrate after 48 h. These results were promising, especially considering the mild reaction conditions used herein (a non-polluting oxidant and 50–55 °C). For *n*-hexane oxidation, the conversion was ca. 7%, with high selectivity for hexan-3-one mainly in the case of the hexadecylamine derived solid, which was 100% selective for this product.

CRediT authorship contribution statement

Gustavo Pimenta Ricci: Investigation, Writing – original draft. **Larissa Oliveira Garcia:** Investigation, Writing – original draft. **Eduardo José Nassar:** Conceptualization, Methodology, Writing – review & editing, Project administration, Funding acquisition. **Shirley Nakagaki:** Conceptualization, Methodology, Writing – review & editing. **João Felipe Stival:** Investigation, Writing – original draft. **Zênis Novaes da Rocha:** Investigation, Writing – original draft. **Miguel Angel Vicente:** Conceptualization, Methodology, Writing – review & editing. **Raquel Trujillano:** Conceptualization, Methodology, Writing – review & editing. **Alejandro Jiménez:** Investigation, Writing – original draft. **Vicente Rives:** Conceptualization, Methodology, Writing – review & editing. **Liziane Marçal:** Conceptualization, Methodology, Writing – review & editing. **Emerson Henrique de Faria:** Conceptualization, Methodology, Writing – review & editing, Project administration, Funding acquisition. **Katia Jorge Ciuffi:** Conceptualization, Methodology, Writing – review & editing, Project administration, Funding

acquisition.

Declaration of competing interest

The authors declare that they have no known competing financial interests or personal relationships that could have appeared to influence the work reported in this paper.

Acknowledgements

The authors thank a Cooperation Grant jointly financed by Universidad de Salamanca (Spain) and FAPESP (Brazil), reference 2016/50322-2. The Brazilian group acknowledges the support from research funding agencies Fundação de Amparo à Pesquisa do Estado de São Paulo, FAPESP (2013/19523-3, 2017/15482-1), and Coordenação de Aperfeiçoamento de Pessoal de Nível Superior (CAPES), Finance code 001, and Conselho Nacional de Desenvolvimento Científico e Tecnológico, CNPq (311767/2015-0, 303135/2018-2 and 305180/2019-3). The equipment of the Brazilian group has been financed by FAPESP (1998/11022-3, 2005/00720-7, 2011/03335-8, 2012/11673-3 and 2016/01501-1).

Appendix A. Supplementary data

Supplementary data to this article can be found online at https://doi.org/10.1016/j.micromeso.2021.111317.

References

[1] G. Centi, S. Perathoner, Catalysis, a driver for sustainability and societal challenges, Catal. Today 138 (2008) 69–76.
[2] F. Cavani, J.H. Teles, Sustainability in catalytic oxidation: an alternative approach or a structural evolution? ChemSusChem 2 (2009) 508–534.
[3] G. Centi, S. Perathoner, Catalysis and sustainable (green) Chemistry, Catal. Today 77 (2003) 287–297.
[4] N.M. Sanchez, A. Klerk, Low-temperature oxidative asphaltenes liquefaction for petrochemicals: fact or fiction? Appl. Petrochem. Res. 6 (2016) 97–106.
[5] X. Tang, X. Jia, Z. Huang, Challenges and opportunities for alkane functionalisation using molecular catalysts, Chem. Sci. 9 (2018) 288–299.
[6] A. Goti, F. Cardona, Hydrogen peroxide in green oxidation reactions: recent catalytic processes, in: P. Tundo, V. Esposito (Eds.), Green Chemical Reactions, NATO Science for Peace and Security Series (Series C: Environmental Security). Springer, 2008.
[7] R.A. Sheldon, Engineering a more sustainable world through catalysis and green chemistry, J. R. Soc. Interface 13 (2016) 20160087.
[8] V. Smeets, A. Styskalik, D.P. Debecker, Non-hydrolytic sol–gel as a versatile route for the preparation of hybrid heterogeneous catalysts, J. Sol. Gel Sci. Technol. 97 (2021) 505–522.
[9] A. Maleki, Z. Hajizadeh, R. Firouzi-Haji, Eco-friendly functionalization of magnetic halloysite nanotube with SO_3H for synthesis of dihydropyrimidinones, Microporous Mesoporous Mater. 259 (2018) 46–53.
[10] M. Azizi, A. Maleki, F. Hakimpoor, Solvent, metal and halogen-free synthesis of sulfoxides by using a recoverable heterogeneous urea-hydrogen peroxide silica-based oxidative catalytic system, Catal. Commun. 100 (2017) 62–65.
[11] D.P. Debecker, P.H. Mutin, Non-hydrolytic sol-gel routes to heterogeneous catalysts, Chem. Soc. Rev. 41 (2012) 3624–3650.
[12] D.P. Debecker, Innovative sol-gel routes for the bottom-up preparation of heterogeneous catalysts, Chem. Rec. 18 (2018) 662–675.
[13] D.P. Debecker, V. Hulea, P.H. Mutin, Mesoporous mixed oxide catalysts via nonhydrolytic sol–gel: a review, Appl. Catal. A Gen. 451 (2013) 192–206.
[14] D. Morselli, F. Bondioli, M. Sangermano, M. Messori, Nano-structured composites prepared by in situ sol-gel synthesis, Polymer 53 (2012) 283–290.
[15] A.M. Cojocariua, P.H. Mutin, E. Dumitriu, A. Aboulaich, A. Vioux, F. Fajula, V. Hulea, Non-hydrolytic SiO_2–TiO_2 mesoporous xerogels—efficient catalysts for the mild oxidation of sulfur organic compounds with hydrogen peroxide, Catal. Today 157 (2010) 270–274.
[16] D.P. Debecker, R. Delaigle, K. Bouchmella, P. Eloy, E.M. Gaigneaux, P.H. Mutin, Total oxidation of benzene and chlorobenzene with MoO_3- and WO_3-promoted V_2O_5/TiO_2 catalysts prepared by a nonhydrolytic sol–gel route, Catal. Today 157 (2010) 125–130.
[17] D.P. Debecker, K. Bouchmella, M. Stoyanova, U. Rodemerck, E.M. Gaigneaux, P. H. Mutin, A non-hydrolytic sol–gel route to highly active MoO_3–SiO_2–Al_2O_3 metathesis catalysts, Catal. Sci. Technol. 2 (2012) 1157–1164.
[18] B.L. Caetano, L.A. Rocha, E. Molina, Z.N. Rocha, G.P. Ricci, P.S. Calefi, O.J. de Lima, C. Mello, E.J. Nassar, K.J. Ciuffi, Cobalt aluminum silicate complexes prepared by the non-hydrolytic sol–gel route and their catalytic activity in hydrocarbon oxidation, Appl. Catal. 311 (2006) 122–134.
[19] S. Acosta, R.J.P. Corriu, D. Leclercq, P. Lefèvre, P.H. Mutin, A. Vioux, Preparation of alumina gels by a non-hydrolytic sol-gel processing method, J. Non-Cryst. Solids 170 (1994) 234–242.
[20] J.N. Hay, H.M. Raval, Preparation of inorganic oxides via a non-hydrolytic sol-gel route, J. Sol. Gel Sci. Technol. 13 (1998) 109–112.
[21] O.J. de Lima, D.P. de Aguirre, D.C. de Oliveira, M.A. da Silva, C. Mello, C.A. P. Leite, H.C. Sacco, K.J. Ciuffi, Porphyrins entrapped in an alumina matrix, J. Mater. Chem. 11 (2001) 2476–2481.
[22] M. Saltarelli, E.H. de Faria, K.J. Ciuffi, E.J. Nassar, R. Trujillano, V. Rives, M. A. Vicente, Aminoiron(III)–porphyrin–alumina catalyst obtained by non-hydrolytic sol-gel process for heterogeneous oxidation of hydrocarbons, Mol Catal 462 (2019) 114–125.
[23] T.C.O. Mac Leod, D.F.C. Guedes, M.R. Lelo, R.A. Rocha, B.L. Caetano, K.J. Ciuffi, M.D. Assis, Catalytic activity of Jacobsen catalyst encapsulated in an alumina matrix by the sol–gel process, J. Mol. Catal. A Chem. 259 (2006) 319–327.
[24] J.M.A. Caiut, S. Nakagaki, O.J. De Lima, C. Mello, C.A.P. Leite, E.J. Nassar, K. J. Ciuffi, H.C. Sacco, Encapsulation of tetraazaannulenato compounds in matrix by sol-gel process, J. Sol. Gel Sci. Technol. 28 (2006) 57–64.
[25] G.P. Ricci, Z.N. Rocha, S. Nakagaki, K.A.D.F. Castro, A.E.M. Crotti, P.S. Calefi, E. J. Nassar, K.J. Ciuffi, Iron-alumina materials prepared by the non-hydrolytic sol-gel route: synthesis, characterization and application in hydrocarbons oxidation using hydrogen peroxide as oxidant, Appl. Catal. A Gen. 389 (2010) 147–154.
[26] Y. Yang, L. Li, Y. Li, J. Rooke, C. Sanchez, B. Su, Hierarchically porous materials: synthesis strategies and structure design, Chem. Soc. Rev. 45 (2017) 481–558.
[27] V. Lafond, P.H. Mutin, A. Vioux, Control of the texture of Titania−Silica mixed oxides prepared by nonhydrolytic Sol−Gel, Chem. Mater. 16 (2004) 5380–5386.
[28] N. Bizaia, E.H. de Faria, G.P. Ricci, P.S. Calefi, E.J. Nassar, K.A.D.F. Castro, S. Nakagaki, K.J. Ciuffi, R. Trujillano, M.A. Vicente, A. Gil, S.A. Korili, Porphyrin−Kaolinite as efficient catalyst for oxidation reactions, ACS Appl. Mater. Interfaces 1 (2009) 2667–2678.
[29] T.E. Cintra, M. Saltarelli, R.M.F. Salmazo, T.H. Silva, E.J. Nassar, R. Trujillano, V. Rives, M.A. Vicente, E.H. de Faria, K.J. Ciuffi, Catalytic activity of porphyrin-catalysts immobilized on kaolinite, Appl. Clay Sci. 168 (2019) 469–477.
[30] M.A. Carreon, V.V. Guliants, Mesostructured vanadium-phosphorus-oxide phases, Microporous Mesoporous Mater. 55 (2002) 297–304.
[31] M. Tiemann, M. Schulz, C. Jaäger, M. Fröba, Mesoporous aluminophosphate molecular sieves synthesized under nonaqueous conditions, Chem. Mater. 13 (2001) 2885–2891.
[32] J. Kim, K. Biswas, K.W. Jhon, S.Y. Jeong, W.S. Ahn, Synthesis of AlPO4-5 and CrAPO-5 using aluminum dross, J. Hazard Mater. 169 (2009) 919–925.
[33] P.H. Mutin, A. Vioux, Nonhydrolytic processing of oxide-based materials: simple routes to control homogeneity, morphology, and nanostructure, Chem. Mater. 21 (2009) 582–596.
[34] F. Rouquerol, J. Rouquerol, K. Sing, Adsorption by Powders and Porous Solids: Principles, Methodology and Applications, Academic Press, 1999.
[35] C. Breen, Thermogravimetric study of the desorption of cyclohexylamine and pyridine from an acid-treated Wyoming bentonite, Clay Miner. 26 (1991) 473–486.
[36] C. Breen, Thermogravimetric and infrared study of the desorption of butylamine, cyclohexylamine and pyridine from Ni and Co exchanged montmorillonite, Clay Miner. 26 (1991) 487–496.
[37] C. Breen, J. Forsyth, J. Yarwood, T. Hughes, Thermal desorption–degradation of cyclohexylamine over Ni^{2+}- and Al^{3+}-exchanged bentonite studied using evolved gas analysis (TG-EGA) and diffuse reflectance spectroscopy (DRIFTS), Phys. Chem. Chem. Phys. 2 (2000) 3887–3892.
[38] A. Steffen, S. Teixeira, J. Sepulveda, R. Rinaldi, U. Schuchardt, Alumina-catalyzed Baeyer-Villiger oxidation of cyclohexanone with hydrogen peroxide, J. Mol. Catal. A Chem. 287 (2008) 41–44.
[39] P. Oliveira, A. Machado, A.M. Ramos, I.M. Fonseca, F.M.B. Fernandes, A.M.B. do Rego, J. Vita, Anchoring manganese acetylacetonate complex on MCM-41: catalytic testing on limonene oxidation, Catal. Commun. 8 (2007) 1366–1372.
[40] S.H. Jhung, J.H. Lee, A.K. Cheetham, G. Férey, J.S. Chang, A shape-selective catalyst for epoxidation of cyclic olefins: the nanoporous nickel phosphate VSB-5, J. Catal. 239 (2006) 97–104.
[41] G.B. Shulpin, G.V. Nizova, Formation of alkyl peroxides in oxidation of alkanes by H_2O_2 catalyzed by transition metal complexes, React, Kinet. Catal. Lett. 48 (1992) 333–338.
[42] G.B. Shul'pin, Metal-catalyzed hydrocarbon oxygenations in solutions: the dramatic role of additives: a review, J. Mol. Catal. A Chem. 189 (2002) 39–66.
[43] S. Vural, Ö. Sari, Synthesis and characterization of SDS assistant α-alumina structures and investigation of the effect of the calcination time on the morphology, Colloid Polym. Sci. 297 (2019) 107–114.
[44] C. Subrahmanyam, B. Viswanathan, T.K. Varadarajan, Synthesis, characterization and catalytic activity of mesoporous trivalent iron substituted aluminophosphates, J. Mol. Catal. A Chem. 223 (2004) 149–153.
[45] P. Tartaj, J. Tartaj, Microstructural evolution of iron-oxide-doped alumina nanoparticles synthesized from microemulsions, Chem. Mater. 14 (2002) 536–541.
[46] I.K. Tonlé, T. Diaco, E. Ngameni, C. Detellier, Nanohybrid kaolinite-based materials obtained from the interlayer grafting of 3-aminopropyltriethoxysilane and their potential use as electrochemical sensors, Chem. Mater. 19 (2007), 6629−2236.
[47] Z.Y. Zhong, T. Prozorov, I. Felner, A. Gedanken, Sonochemical synthesis and characterization of iron oxide coated on submicrospherical Alumina: A direct observation of interaction between iron oxide and alumina, J. Phys. Chem. 103 (1999) 947–956.
[48] J. Leivo, M. Lindén, J.M. Rosenholm, M. Ritola, C.V. Teixeira, E. Levänen, T. A. Mäntylä, Evolution of aluminosilicate structure and mullite crystallization from

homogeneous nanoparticulate sol–gel precursor with organic additives, J. Eur. Ceram. Soc. 28 (2008) 1749–1762.
[49] A. Jitianu, M. Crisan, A. Meghea, I. Rau, M. Zaharescu, Influence of the silica based matrix on the formation of iron oxide nanoparticles in the Fe_2O_3–SiO_2 system, obtained by sol–gel method, J. Mater. Chem. 12 (2002) 1401–1407.
[50] M. Thommes, K. Kaneko, A.V. Neimark, J.P. Olivier, F. Rodriguez-Reinoso, J. Rouquerol, K.S.W. Sing, Physisorption of gases, with special reference to the evaluation of surface area and pore size distribution (IUPAC Technical Report), Pure Appl. Chem. 87 (2015) 1051–1069.
[51] J. Yin, X. Zhao, Wormhole-like mesoporous Ce-doped TiO_2: a new electrorheological material with high activity, J. Mater. Chem. 13 (2003) 689–695.
[52] J. Aguado, J.M. Escola, M.C. Castro, Influence of the thermal treatment upon the textural properties of sol–gel mesoporous γ-alumina synthesized with cationic surfactants, Microporous Mesoporous Mater. 128 (2010) 48–55.
[53] A. De Stefanis, S. Kaciulis, L. Pandolfi, Preparation and characterization of Fe-MCM-41 catalysts employed in the degradation of plastic materials, Microporous Mesoporous Mater. 99 (2007) 140–148.
[54] R. Rinaldi, U. Schuchardt, On the paradox of transition metal-free alumina-catalyzed epoxidation with aqueous hydrogen peroxide, J. Catal. 236 (2005) 335–345.
[55] L.H. Song, S.B. Park, Synthesis of mesoporous Fe-incorporated alumina particles with regular pores, Mater. Lett. 65 (2011) 1850–1852.
[56] K.A.D.F. Castro, M. Halma, G.S. Machado, G.P. Ricci, G.M. Ucoski, K.J. Ciuffi, S. Nakagaki, Preparation of catalysts based on iron(III) porphyrins heterogenized on silica obtained by the sol-gel process for hydroxylation and epoxidation reactions, J. Braz. Chem. Soc. 21 (2010) 1329–1340.
[57] F.J. Luna, U. Schuchardt, Modificação de zeólitas para uso em catálise, Quim. Nova 24 (2001) 885–892.
[58] S. Bordiga, R. Buzzoni, F. Geobaldo, C. Lamberti, E. Giamello, A. Zecchina, G. Leofanti, G. Petrini, G. Tozzola, G. Vlaic, Structure and reactivity of framework and extraframework iron in Fe-silicalite as investigated by spectroscopic and physicochemical methods, J. Catal. 158 (1996) 486–501.
[59] H. Xin, J. Liu, F. Fan, Z. Feng, G. Jia, Q. Yang, C. Li, Mesoporous ferrosilicates with high content of isolated iron species synthesized in mild buffer solution and their catalytic application, Microporous Mesoporous Mater. 113 (2008) 231–239.
[60] Y. Yu, G. Xiong, C. Li, F.S. Xiao, Characterization of iron atoms in the framework of MFI-type zeolites by UV resonance Raman spectroscopy, J. Catal. 194 (2000) 487–490.
[61] R. Rinaldi, F.Y. Fujiwara, W. Hölderich, U. Schuchardt, Tuning the acidic properties of aluminas via sol-gel synthesis: new findings on the active site of alumina-catalyzed epoxidation with hydrogen peroxide, J. Catal. 244 (2006) 92–101.
[62] R. Rinaldi, F.Y. Fujiwara, U. Schuchardt, Chemical and physical changes related to the deactivation of alumina used in catalytic epoxidation with hydrogen peroxide, J. Catal. 245 (2007) 456–465.
[63] D.H.R. Barton, B. Hu, The selective functionalization of saturated hydrocarbons: recent developments in Gif chemistry, Pure Appl. Chem. 69 (1997) 1941–1950.
[64] J.T. Groves, High-valent iron in chemical and biological oxidations, J. Inorg. Biochem. 100 (2006) 434–447.
[65] F. Gozzo, Radical and non-radical chemistry of the Fenton-like systems in the presence of organic substrates, J. Mol. Catal. A Chem. 171 (2001) 1–22.
[66] H.B. Dunford, Oxidations of iron(II)/(III) by hydrogen peroxide: from aquo to enzyme, Coord. Chem. Rev. 233–234 (2002) 311–318.
[67] G.S. Nunes, A.D.P. Alexiou, H.E. Toma, Catalytic oxidation of hydrocarbons by trinuclear μ-oxo-bridged ruthenium-acetate clusters: radical versus non-radical mechanisms, J. Catal. 260 (2008) 188–192.
[68] I.W.C.E. Arends, R.A. Sheldon, Activities and stabilities of heterogeneous catalysts in selective liquid phase oxidations: recent developments, Appl. Catal. 212 (2001) 175–187.
[69] M. Selvaraj, D.-W. Park, C.S. Há, Well ordered two-dimensional mesoporous CeSBA-15 synthesized with improved hydrothermal stability and catalytic activity, Microporous Mesoporous Mater. 138 (2011) 94–101.
[70] X. Liu, J. He, L. Yang, Y. Wang, S. Zhang, W. Wang, J. Wang, Liquid-phase oxidation of cyclohexane to cyclohexanone over cobalt-doped SBA-3, Catal. Commun. 11 (2010) 710–714.
[71] A. Ramanathan, M.S. Hamdya, R. Parton, T. Maschmeyer, J.C. Jansen, U. Hanefeld, Co-TUD-1 catalysed aerobic oxidation of cyclohexane, Appl. Catal. A Gen. 355 (2009) 78–82.
[72] E.A. Mikhalyova, O.V. Makhlynets, T.D. Palluccio, A.S. Filatov, E.V. Rybak-Akimova, A new efficient iron catalyst for olefine poxidation with hydrogen peroxide, Chem. Commun. 48 (2012) 687–689.
[73] E.H. de Faria, G.P. Ricci, L. Marçal, E.J. Nassar, M.A. Vicente, R. Trujillano, A. Gil, S.A. Korili, K.J. Ciuffi, P.S. Calefi, Green and selective oxidation reactions catalyzed by kaolinite covalently grafted with Fe (III) pyridine-carboxylate complexes, Catal. Today 187 (2012) 135–149.
[74] J.M. Thomas, R. Raja, G. Sankar, R.G. Bell, Molecular-sieve catalysts for the selective oxidation of linear alkanes by molecular oxygen, Nature 398 (1999) 227–230.
[75] R. Raja, J.M. Thomas, Catalyst design strategies for controlling reactions in microporous and mesoporous molecular-sieves, J. Mol. Catal. A Chem. 181 (2002) 3–14.